Structural properties and superconductivity of $SrFe_2As_{2-x}P_x$ ($0.0 \leq x \leq 1.0$) and $CaFe_2As_{2-y}P_y$ ($0.0 \leq y \leq 0.3$)

2010 J. Phys.: Condens. Matter 22 125702

(http://iopscience.iop.org/0953-8984/22/12/125702)

J. Phys.: Condens. Matter **22** (2010) 125702 (6pp) doi:10.1088/0953-8984/22/12/125702

Structural properties and superconductivity of $SrFe_2As_{2-x}P_x$ ($0.0 \leqslant x \leqslant 1.0$) and $CaFe_2As_{2-y}P_y$ ($0.0 \leqslant y \leqslant 0.3$)

H L Shi, H X Yang, H F Tian, J B Lu, Z W Wang, Y B Qin, Y J Song and J Q Li[1]

Beijing National Laboratory for Condensed Matter Physics, Institute of Physics, Chinese Academy of Sciences, Beijing 100190, People's Republic of China

E-mail: LJQ@aphy.iphy.ac.cn

Received 8 October 2009, in final form 24 January 2010
Published 11 March 2010
Online at stacks.iop.org/JPhysCM/22/125702

Abstract

The $SrFe_2As_{2-x}P_x$ ($0.0 \leqslant x \leqslant 1.0$) and $CaFe_2As_{2-y}P_y$ ($0.0 \leqslant y \leqslant 0.3$) materials were prepared by a solid-state reaction method. X-ray diffraction measurements indicate that the single-phase samples can be successfully obtained for $SrFe_2As_{2-x}P_x$ ($0.0 \leqslant x \leqslant 0.8$) and $CaFe_2As_{2-y}P_y$ ($0.0 \leqslant y \leqslant 0.3$). Visible contraction of the lattice parameters is determined due to the relatively smaller radius of P ions in comparison with that of As. The spin-density-wave (SDW) instability associated with the tetragonal to orthorhombic phase transition is suppressed noticeably in both systems following the increase in P content. The highest superconducting transitions are observed at about 27 K in $SrFe_2As_{1.3}P_{0.7}$ and at about 13 K in $CaFe_2As_{1.925}P_{0.075}$, respectively. Structural analysis suggests that lattice contraction could notably affect the superconductivity in these materials.

1. Introduction

Following the discovery of superconductivity at $T_c \approx 26$ K in LaFeAsO(F) [1], a variety of isostructural compounds were synthesized under different conditions, such as RTMPO (R = rare earth metal, TM = transition metal) [2–4], RTMAsO [5–12] and SrFeAsF [13] (the so-called 1111 type). These materials could exhibit numerous interesting physical properties, e.g. ferromagnetism (FM), antiferromagnetism (AFM), spin density waves (SDW) and superconductivity. Similar structural and physical phenomena have also been observed in the AFe_2As_2 materials (A = Ca, Sr, Ba, Eu, so-called 122 type) [14–19]. Electron or hole doping [20–23] in a number of systems can suppress the SDW and result in superconductivity in both the 1111 and 122 materials. Recent experimental investigations revealed that the P substitution for As in $BaFe_2As_2$ could also induce superconductivity as high as ~31 K [24]. Theoretical calculations [25] suggest that P substitution for As does not result in significant changes in the electron density, but shows clear influence on the location of hybridized states, bandwidth and the topography of the Fermi surface. Therefore, the effects of P substitution for As on the physical properties, especially superconductivity in the related systems, are still a interesting issue in recent investigations. In this paper, a series of single-phase polycrystalline samples of $SrFe_2As_{2-x}P_x$ and $CaFe_2As_{2-y}P_y$ have been prepared, and the highest superconducting critical temperature T_c is obtained at about 27 K in $SrFe_2As_{1.3}P_{0.7}$ and at 13 K in $CaFe_2As_{1.925}P_{0.075}$ material, respectively. Our careful structural studies suggest that local structural features in the Fe–As layers could evidently influence the physical properties of these materials [25].

2. Experimental details

Polycrystalline samples of $SrFe_2As_{2-x}P_x$ ($0.0 \leqslant x \leqslant 1.0$) and $CaFe_2As_{2-y}P_y$ ($0.0 \leqslant y \leqslant 0.3$) were synthesized by the solid-state reaction as reported in previous literature [16, 23].

[1] Author to whom any correspondence should be addressed.

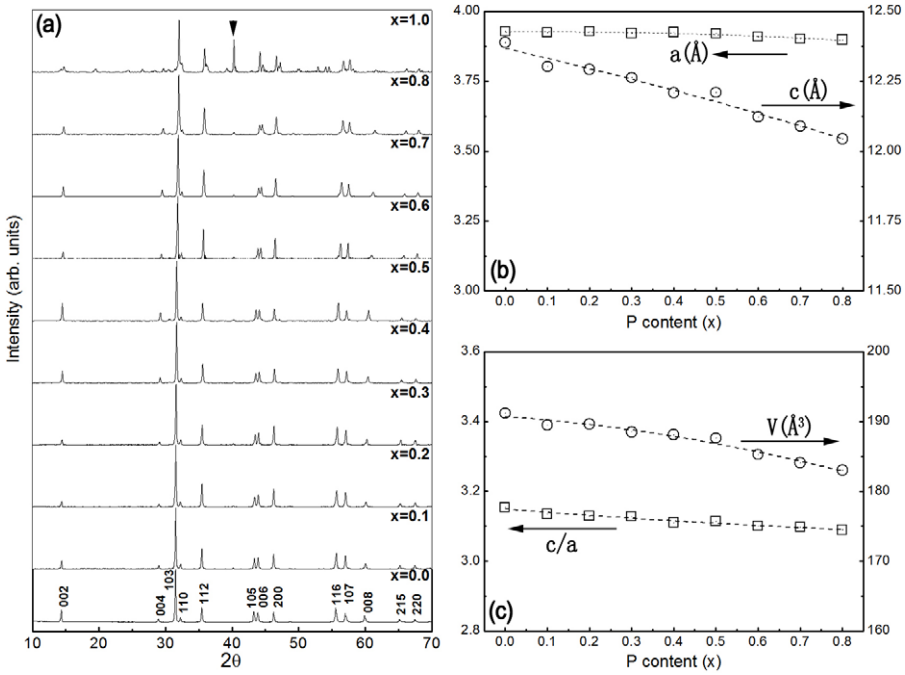

Figure 1. (a) X-ray diffraction patterns of $SrFe_2As_{2-x}P_x$ ($x = 0$–1.0), where peaks of the impurity phase are strengthened with the increase in phosphorus content, which is marked by an arrow; (b) and (c) lattice parameters as a function of P content.

The starting materials of $Ca(Sr)Fe_2As_2$ and $Ca(Sr)Fe_2P_2$ were prepared by using small Ca or Sr chunks and the high quality of Fe, As and P powders. The mixtures with the desired compositions are pressed into pellets, placed in a small alumina crucible, and then sealed in a silica tube, each tube filled with 1/3 argon gas. The tube was then heated at 800 °C for 24 h and then cooled down to room temperature. The obtained products were ground down as starting materials. $SrFe_2As_{2-x}P_x$ and $CaFe_2As_{2-y}P_y$ materials were ground and pelleted, and sealed in vacuum tubes which were heated at 850 °C for 48 h and cooled down to room temperature in 12 h. X-ray diffraction (XRD) measurements for all samples were carried out on a diffractometer in the Bragg–Brentano geometry using Cu Kα radiation. Magnetization measurements as a function of temperature were performed using a commercial Quantum Design SQUID. The resistivity (R) as a function of temperature was measured by the standard four-point probe technique.

3. Results

3.1. Structural and physical properties of $SrFe_2As_{2-x}P_x$

Figure 1(a) shows the x-ray diffraction (XRD) patterns of the $SrFe_2As_{2-x}P_x$ ($0.0 \leqslant x \leqslant 1.0$) materials. Structural analysis reveals that the experimental results for the samples with $x < 0.3$ could be well indexed on the basis of a tetragonal $ThCr_2Si_2$-type structure with a space group of $I4/mmm$ (no. 139, $Z = 2$). Peaks of the impurity phase, as marked by the arrow in the diffraction pattern, appear progressively following the increase of P content in addition to the main 122 phase; samples with $x \geqslant 0.8$ are found not to be stable and often decompose in the moist air in several days. Figures 1(b) and (c) show the lattice parameters as a function of P content, illustrating the c-axis parameter and volume of the unit cell decreases gradually with the increase in P content due to the relatively smaller atomic radius of P (98 pm) in comparison with that of As (114 pm). This fact suggests an effective chemical substitution of P for As in our experiments. The experimental data for lattice parameters are listed in table 1.

Table 1. Lattice parameters a, c, c/a ratio and unit cell volumes of $SrFe_2As_{2-x}P_x$ and $CaFe_2As_{2-y}P_y$.

Sample	Content (x/y)	a (Å)	c (Å)	c/a	V (Å^3)
$SrFe_2As_{2-x}P_x$	0.0	3.928(4)	12.388(8)	3.1536(5)	191.188(0)
	0.1	3.924(6)	12.303(2)	3.1348(9)	189.499(9)
	0.2	3.927(6)	12.292(3)	3.1297(2)	189.621(5)
	0.3	3.920(9)	12.262(7)	3.1275(2)	188.520(1)
	0.4	3.925(2)	12.208(8)	3.1103(6)	188.103(4)
	0.5	3.920(0)	12.210(0)	3.1148(0)	187.623(7)
	0.6	3.909(3)	12.122(7)	3.1009(9)	185.266(7)
	0.7	3.902(2)	12.089(1)	3.0980(2)	184.082(7)
	0.8	3.898(3)	12.043(3)	3.0893(7)	183.018(9)
$CaFe_2As_{2-y}P_y$	0.000	3.889(3)	11.701(2)	3.0085(6)	177.001(0)
	0.025	3.899(6)	11.706(3)	3.0019(2)	178.016(3)
	0.050	3.901(3)	11.748(1)	3.0113(3)	178.807(8)
	0.075	3.898(8)	11.691(5)	2.9987(4)	177.718(3)
	0.100	3.897(9)	11.677(3)	2.9957(9)	177.420(5)
	0.125	3.898(8)	11.679(2)	2.9955(9)	177.531(3)
	0.150	3.900(7)	11.684(7)	2.9955(4)	177.788(1)
	0.175	3.899(4)	11.66(8)	2.9922(6)	177.415(7)
	0.200	3.898(9)	11.656(3)	2.9896(4)	177.192(3)
	0.250	3.900(1)	11.695(7)	2.9988(2)	177.900(7)

Figure 2(a) presents the temperature-dependent resistivity for the $SrFe_2As_{2-x}P_x$ samples. Each R–T curve is normalized by its maximum value to facilitate the illustration

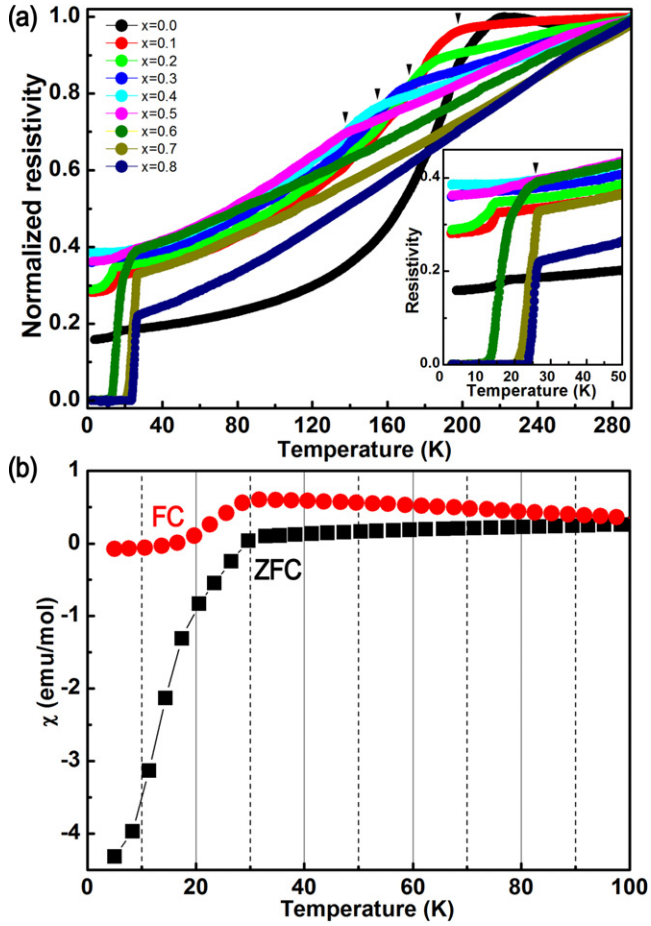

Figure 2. (a) Resistivity as a function of temperature for $SrFe_2As_{2-x}P_x$ samples, demonstrating that SDW is gradually suppressed on increase in P content, where the critical temperature is marked by an arrow. The inset shows the exaggerated curve in the low-temperature range. (b) Magnetic susceptibility for the $x = 0.7$ sample, where $T_{c-onset}$ is at about 30 K.

Table 2. Lattice parameters and $z_{As/P}$ for typical 122 materials.

Sample	a (Å)	c (Å)	$z_{As/P}$
$CaFe_2As_2$ [26]	3.890(8)	11.727(8)	0.366 42
$SrFe_2As_2$ [26]	3.921(8)	12.337(3)	0.3612
$BaFe_2As_2$ [16]	3.957(0)	12.968(5)	0.3545
$CaFe_2P_2$ [27]	3.642(4)	9.485(1)	0.364 33
$SrFe_2P_2$ [27]	3.825(1)	11.612(1)	0.352 18
$BaFe_2P_2$ [27]	3.840(1)	12.442(1)	0.345 64
$CaNi_2As_2$ [33]	4.065(1)	9.949(2)	0.3698
$SrFe_2As_2$ [33]	4.154(1)	10.290(2)	0.362 32
$BaNi_2As_2$ [34]	4.112	11.54	0.3476

of resistivity changes accompanying the SDW instability and superconducting transition. For the parent phase, the pronounced resistivity anomaly at 220 K is considered as arising from the structural phase transition from tetragonal ($I4/mmm$) to orthorhombic phase ($Fmmm$) in association with SDW instability. The SDW anomaly is significantly suppressed with P substitution for As and moves to lower temperatures. For instance, the SDW in the $x = 0.5$ sample

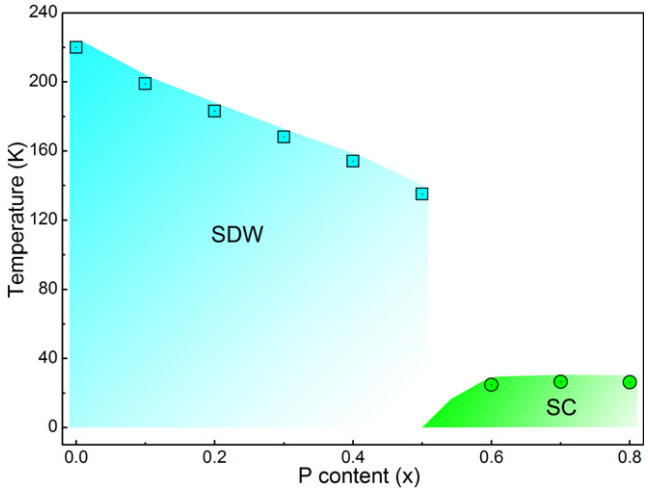

Figure 3. The electronic phase diagram of $SrFe_2As_{2-x}P_x$, showing the structural and superconducting transitions as a function of phosphorus content. Transition temperatures are determined from resistivity measurements using the intersection point of two lines' method.

becomes almost invisible and shows a clear down-turn in resistivity at about 20 K, while the $x = 0.6$ sample shows a linear resistivity in the temperature range from 300 down to 30 K and undergoes a superconducting transition at about 27 K. Further increase in the P content leads to the appearance of an impurity phase in the samples and no obvious increase of T_c is observed. Our careful analysis of $SrFe_2As_{2-x}P_x$ suggests that the highest $T_{c-onset}$ is about 27 K, while T_{c-zero} is about 23 K for P content of around 0.8. Figure 2(b) shows the experimental results of magnetization, demonstrating a clear superconducting transition just below 30 K for the $x = 0.7$ sample. It should be noted that, for the underdoped samples, there is an obvious down-turn at about 18 K and is weakened on increasing P content, which should be considered as a surface or filamentary effect, likely due to the strain, as reported in the previous literature [28, 32].

The electronic phase diagram for the $SrFe_2As_{2-x}P_x$ samples is plotted in figure 3, where the onset $T_{c-onset}$ and T_{SDW} are estimated from resistivity measurements using the intersection point of two lines' method, and P content is adopted from the nominal data although a slight deviation is present possibly in the samples with $x > 0.7$. Systematic analysis on the experimental results indicates that the suppression of SDW in $SrFe_2As_{2-x}P_x$ is rather moderate compared with the Co substitution in $SrFe_{2-x}Co_xAs_2$ materials. This is due to the P substitution for As being not directly on the Fe site which plays a critical role for SDW and superconductivity in the present system.

3.2. Structural and physical properties of $CaFe_2As_{2-y}P_y$

The $CaFe_2As_{2-y}P_y$ ($y = 0.0$–0.3) polycrystalline samples have been successfully synthesized using a similar preparation route. We also make numerous attempts to prepare samples for P contents ranging from 0.3 to 1.0. These samples in general are rather unstable and tend to decompose in the moist air, just

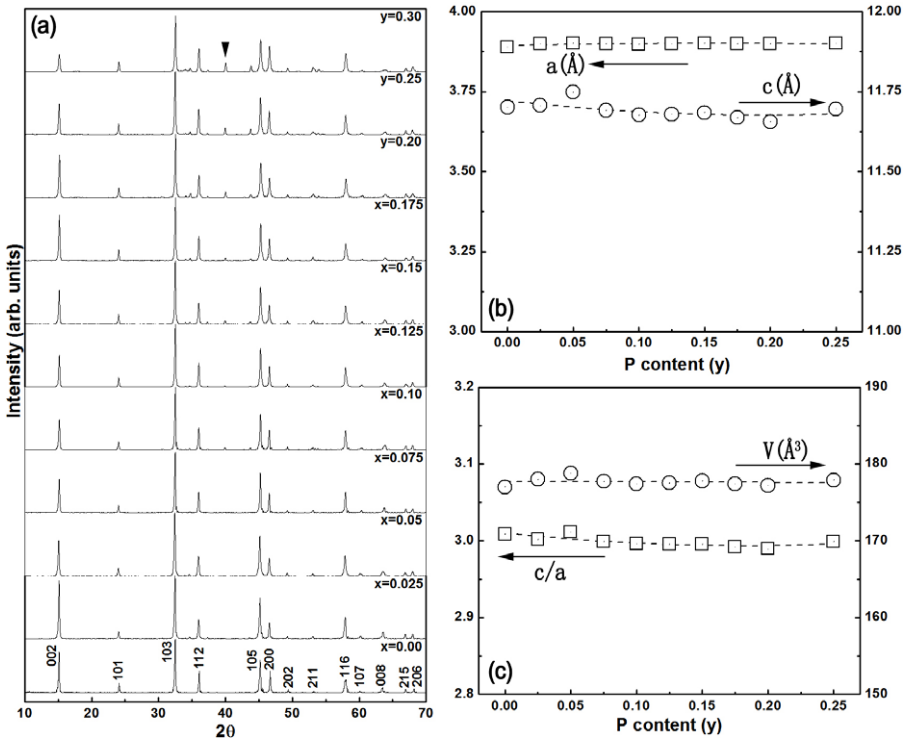

Figure 4. (a) X-ray diffraction patterns of $CaFe_2As_{2-y}P_y$ samples ($y = 0$–0.3), where a peak from an impurity phase is marked by an arrow; (b) and (c) lattice parameters as a function of phosphorus content.

like the case of $SrFe_2As_{2-x}P_x$ with $x > 0.8$. Figure 4(a) presents the x-ray diffraction patterns, in which the main reflection peaks can be well indexed with the tetragonal phase $I4/mmm$, except for the additional peaks of the impurity phase between the 112 and 105 peaks for the samples with $y \geqslant 0.10$. Figures 4(b) and (c) show the lattice parameters as a function of phosphorus content, indicating the visible contraction of lattice parameters due to the relatively small size of the P ion in comparison with that of As. The experimental data of lattice parameters are listed in table 1.

Figure 5(a) shows the temperature dependence of the normalized resistivity curve, it is recognizable that a small amount of P ($y = 0.025$) could drastically suppress the SDW from 145 K down to $T_{SDW} \approx 120$ K and a visible downturn of resistivity appears at about 13 K. When phosphorus content is up to $y = 0.075$, the SDW phase transition becomes almost invisible and a clear drop in resistivity occurs at about 13 K, but zero resistivity is not reached down to 4 K. Further increase of the P content could not visibly improve the superconducting T_c. Magnetization measurements indicate that a significant diamagnetic signal is obtained at about 11 K, suggesting this resistivity drop corresponds to a superconducting transition. However, notably a ferromagnetic background signal is often observed, which possibly results from the impurity phases which induce the residual resistivity below the superconducting transition.

4. Discussion

Actually, the effect of structural alterations on the physical properties as an important issue has been extensively investigated for the Fe-based superconductors in the previous literature. Theoretical investigations on the $BaFe_2As_2$ [25] suggest that the Fermi surface could be evidently influenced by the P substitution for As. Substitution of P for As into the Fe–As layer does not yield additional electrons or holes in the system, but the visible changes of local structures can be observed, such as the As/P ionic positions in the unit cell (z_{As} and z_P). These changes can evidently influence the bandwidth, location of hybridized states and topography of the Fermi surface [30]. For instance, the isovalent substitution of As with P in $EuFe_2As_2$ was found to result in clear superconducting transitions [31]. Careful structural investigations of $EuFe_2As_{0.7}P_{0.3}$ demonstrated that the P doping yields a closer distance between As/P and Fe planes, which can generate chemical pressure as manifested by the shrinkage of the lattice. Superconductivity appearing in $EuFe_2As_{0.7}P_{0.3}$ in comparison with that observed in $EuFe_2As_2$ under hydrostatic pressure often shows the onset transition of a resistivity drop at the same temperature. This fact suggests that the effect of internal chemical pressure could be analogous to the application of external physical pressure. From electronic structural points of view, the P position ($z_{As/p}$) in a 1111-type structure [29] can significantly affect the hole pocket around the Γ-point at the Fermi surface and is considered to be a key factor for the change of high-T_c nodeless to low-T_c nodal pairing. For the parent compound of the 122 phase, the hole pocket around the Γ-point shows clear quasi-two-dimensional features. When As is completely substituted by P, this hole pocket shows clear three-dimensional features [37]. It is possible that $z_{As/P}$ acts in a similar role to affect the topography of hole and hopping integrals.

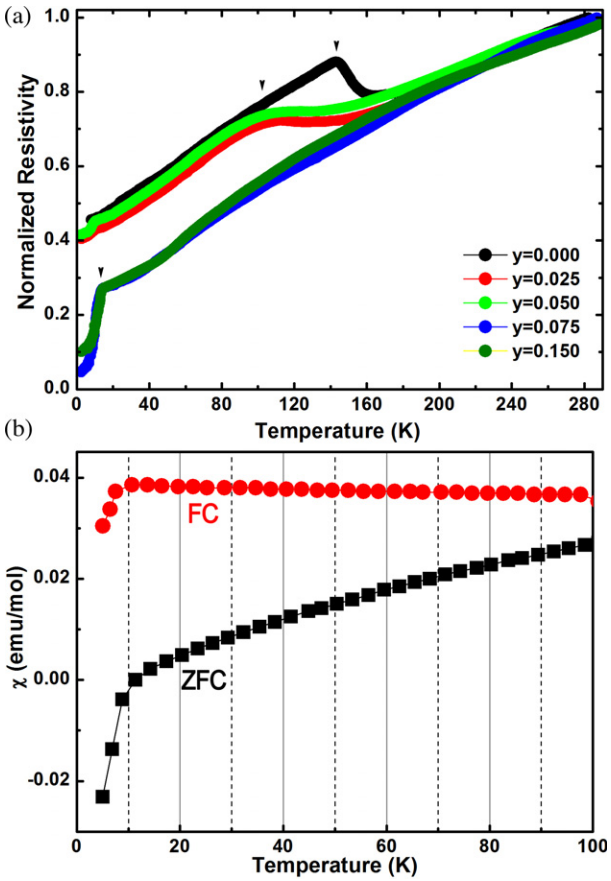

Figure 5. (a) Resistivity as a function of temperature for $CaFe_2As_{2-y}P_y$ samples, where the critical temperature is marked by arrows; (b) magnetic susceptibility for $y = 0.075$ samples.

On the other hand, experimental investigations [35] suggest that systematically replacing R from La to Ce, Pr, Nd and Sm in $RFeAsO_{1-\delta}$ leads a gradual decrease in the a-axis lattice parameters and increase in T_c. It was also pointed out that a systematic correlation between superconducting T_c and the Fe–As–Fe bond angles is expected because the exchange couplings (J_1 and J_2) and the electronic bandwidth W are directly related to the Fe–As–Fe bond angles [36]. Our recent investigations [26, 27, 33, 34] demonstrate that the 3d electron doping or P substitution for As could significantly affect the local structural properties of 122 materials. Figure 6 shows the variations of bond lengths of Fe–As(P) and bond angles of Fe–As(P)–Fe. In comparison with the $BaFe_2As_2$ system, the bond lengths of Fe–As and bond angles of Fe–As–Fe in $CaFe_2As_2$ are decreased smoothly and both materials exhibit well 2D (or quasi-2D) features. On the other hand, bond lengths of Fe–P in $CaFe_2P_2$ are drastically contracted in comparison with those in $BaFe_2P_2$, and bond angles of Fe–P–Fe are significantly increased. The presence of metallic Ca–P bonding can visibly influence the location of hybridized states at the Fermi surface and yields certain 3D behaviors in $CaFe_2P_2$ [37]. A similar property was also observed in the ANi_2As_2 system in which the bonding angles in $CaNi_2As_2$ are drastically contracted in comparison with $BaNi_2As_2$ and $SrNi_2As_2$ materials, which makes this material more three-dimensional. A small amount of Ni or P doping in the present case was found to create great variation in both structural and physical properties.

5. Conclusions

We have successfully prepared a series of $SrFe_2As_{2-x}P_x$ ($0.0 \leqslant x \leqslant 1.0$) and $CaFe_2As_{2-y}P_y$ ($0.0 \leqslant y \leqslant 0.3$) samples using the conventional solid-state reaction method. Continuous reduction of lattice parameters following the increase of the P content shows that P atoms are effectively substituted for As in

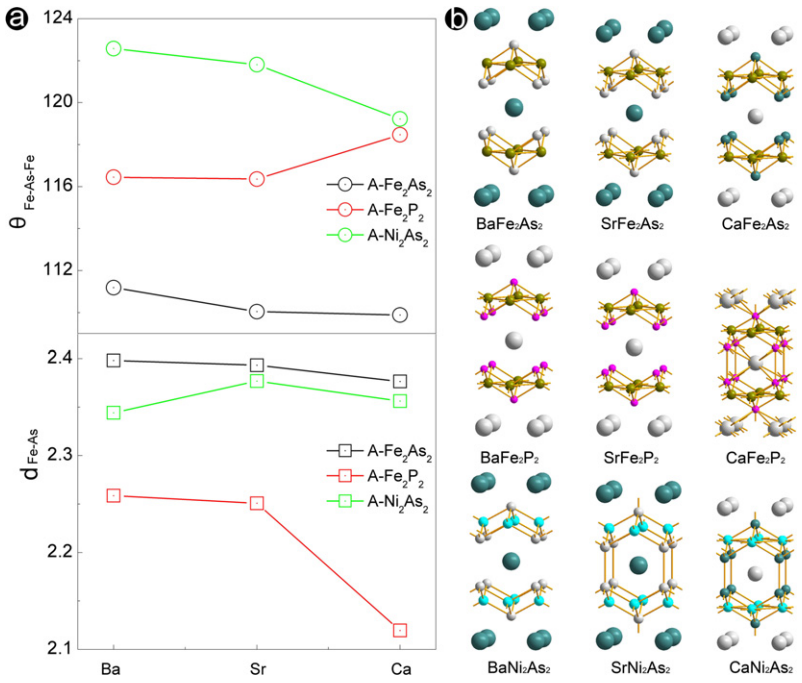

Figure 6. (a) Bond lengths of Fe–As(P) and bond angles of Fe–As(P)–Fe in AFe_2As_2, AFe_2P_2 and ANi_2As_2 systems; (b) atomic structural models for the 122 systems.

our samples. Certain samples with relatively high P content are rather unstable and often decompose into powders in a few days. The resistivity anomaly associated with the SDW instability is suppressed with the P substitution for As. Clear superconducting transitions were observed in $SrFe_2As_{1.3}P_{0.7}$ at 27 K and $CaFe_2As_{1.925}P_{0.075}$ at 13 K. Structural analysis suggests that the lattice contraction plays a significant role in the appearance of superconductivity in the 122 system.

Acknowledgments

We would like to thank W W Huang for dc-magnetization measurements. This work is supported by the National Science Foundation of China, the Knowledge Innovation Project of the Chinese Academy of Sciences and the 973 projects of the Ministry of Science and Technology of China.

References

[1] Kamihara Y, Watanabe T, Hirano M and Hosono H 2008 *J. Am. Chem. Soc.* **130** 3296
[2] Kamihara Y, Hiramatsu H, Hirano M, Kawamura R, Yanagi H, Kamiya T and Hosono Hi 2006 *J. Am. Chem. Soc.* **128** 10012
[3] Baumbach R E, Hamlin J J, Shu L, Zocco D A, Crisosto N M and Maple M B 2009 *New J. Phys.* **11** 025018
[4] Watanabe T, Yanagi H, Kamiya T, Kamihara Y, Hiramatsu H, Hirano M and Hosono H 2007 *Inorg. Chem.* **46** 7719
[5] Chen G F *et al* 2008 *Phys. Rev. Lett.* **101** 057007
[6] Chen G F, Li Z, Wu D, Li G, Hu W Z, Dong J, Zheng P, Luo J L and Wang N L 2008 *Phys. Rev. Lett.* **100** 247002
[7] Ren Z A, Yang J, Lu W, Yi W, Che G C, Dong X L, Sun L L and Zhao Z X 2008 *Mater. Res. Innov.* **12** 105
[8] Ren Z A *et al* 2008 *Europhys. Lett.* **82** 57002
[9] Chen X H, Wu T, Wu G, Liu R H, Chen H and Fang D F 2008 *Nature* **453** 761
[10] Cheng P, Fang L, Yang H, Zhu X Y, Mu G, Luo H Q, Wang Z S and Wen H H 2008 *Sci. Chin.* G **51** 719
[11] Li L J, Li Y K, Ren Z, Luo Y K, Lin X, He M, Tao Q, Zhu Z W, Cao G H and Xu Z A 2008 *Phys. Rev.* B **78** 132506
[12] Ren Z A *et al* 2008 *Chin. Phys. Lett.* **25** 2215
[13] Han F, Zhu X Y, Mu G, Cheng P and Wen H H 2008 *Phys. Rev.* B **78** 180503(R)
[14] Ni N, Nandi S, Kreyssig A, Goldman A I, Mun E D, Bud'ko S L and Canfield P C 2008 *Phys. Rev.* B **78** 014523
[15] Yan J Q *et al* 2008 *Phys. Rev.* B **78** 024516
[16] Marianne R, Marcus T and Dirk J 2008 *Phys. Rev.* B **78** 020503
[17] Ren Z, Zhu Z W, Jiang S, Xu X F, Tao Q, Wang C, Feng C M, Cao G H and Xu Z A 2008 *Phys. Rev.* B **78** 052502
[18] Su Y *et al* 2009 *Phys. Rev.* B **79** 064504
[19] Ma C, Yang H X, Tian H F, Shi H L, Lu J B, Wang Z W, Zeng L J, Chen G F, Wang N L and Li J Q 2009 *Phys. Rev.* B **79** 060506
[20] Li Y K *et al* 2009 *Phys. Rev.* B **79** 054521
[21] Sefat A S, Jin R Y, McGuire M A, Sales B C, Singh D J and Mandrus D 2008 *Phys. Rev. Lett.* **101** 117004
[22] Li L J *et al* 2009 *New J. Phys.* **11** 025008
[23] Rotter M, Tegel M and Johrendt D 2008 *Phys. Rev. Lett.* **101** 107006
[24] Jiang S, Xing H, Xuan G F, Wang C, Ren Z, Feng C M, Dai J H, Xu Z A and Cao G H 2009 *J. Phys.: Condens. Matter* **21** 382203
[25] Hashimoto K *et al* 2009 arXiv:0907.4399v1
[26] Tompsett D A and Lonzarich G G 2009 arXiv:0902.4859v2
[27] Mewis A *et al* 1980 *Z. Naturf.* B **35** 141
[28] Saha S R, Butch N P, Kirshenbaum K and Paglione J 2009 *Phys. Rev. Lett.* **103** 037005
[29] Kuroki K, Usui H, Onari S, Arita R and Aoki H 2009 *Phys. Rev.* B **79** 224511
[30] Kasahara S, Shibauchi T, Hashimoto K, Ikada K, Tonegawa S, Ikeda H, Takeya H, Hirata K, Terashima T and Matsuda Y 2009 arXiv:0905.4427v1
[31] Ren Z, Tao Q, Jiang S, Feng Ch M, Wang C, Dai J H, Cao G H and Xu Z A 2009 *Phys. Rev. Lett.* **102** 137002
[32] Saha S R, Butch N P, Kirshenbaum K, Paglione J and Zavalij P Y 2009 *Phys. Rev. Lett.* **103** 37005
[33] Mewis A and Distler A Z 1980 *Z. Naturf.* B **35B** 391
[34] Subedi A and Singh D J 2008 *Phys. Rev.* B **78** 132511
[35] Ren Z A *et al* 2008 *Europhys. Lett.* **83** 17002
[36] Zhao J, Huang Q, de La Cruz C, Li S, Lynn J W and Chen Y 2008 *Nat. Mater.* **7** 953
[37] Coldea A I, Andrew C M J, Analytis J G, McDonald R D, Bangura A F, Chu J H, Fisher I R and Carrington A 2009 *Phys. Rev. Lett.* **103** 026404